On the Efficiency of Horizontal Diffusion and Numerical Filtering in an Arakawa-Type Model

Erich Roeckner and Hans v. Storch
Meteorologisches Institut der Universität Hamburg, F.R.G.

[Original manuscript received 13 November 1979; in revised form 29 February 1980]

ABSTRACT *In a series of 5-day forecasts with a 3-layer/2.8° hemispheric model, horizontal diffusion schemes of the second and fourth degree are compared with a numerical filter technique. The results, which are discussed mainly in terms of spectral energetics in zonal wavenumber space, indicate that fourth-degree diffusion is more scale selective than second-degree and equivalent to filtering. The seventh-order filter applied only intermittently to the prognostic variables is superior to fourth-degree diffusion from the viewpoint of computational economy. Excessive dissipation of the long waves may inhibit the production of eddy kinetic energy from eddy available potential energy.*

RÉSUMÉ *Des algorithmes de diffusion horizontale au deuxième et au quatrième ordres sont comparés à un filtre numérique, sur une série de prédictions de cinq jours chacune, fournie par un modèle hémisphérique 3 couches/2.8°. Les résultats, discutés principalement en termes d'énergie spectrale en espace de nombre d'ondes zonales, indiquent que la diffusion au quatrième ordre sélectionne les échelles plus que ne le fait la diffusion au deuxième ordre et est équivalente à un filtrage. Le filtre de septième ordre appliqué de façon intermittente aux variables du modèle est meilleur que la diffusion au quatrième ordre en ce qui concerne le coût de calcul. Une dissipation excessive des grandes longueurs d'ondes peut réduire la production d'énergie cinétique turbulente à partir de l'énergie turbulente potentielle disponible.*

1 Introduction

Numerical models of atmospheric flow generally show tendency for systematically accumulating energy at the high wavenumber end of the truncated spectrum. The main reasons for this model defect are:

- aliasing error produced by the non-linearity of the governing equations;
- computational modes generated eventually by finite differencing;
- parameterizations of subgrid-scale processes, such as convection or turbulent mixing.

ATMOSPHERE-OCEAN 18 (3) 1980, 239–253 0705-5900/80/0000–0239$01.25/0

Other possible sources of fictitious small-scale energy (noise) production are the boundary conditions and the initial imbalances between the mass and wind fields giving rise to excessive gravitational modes. Numerical instability that might be produced by these effects is generally avoided by introducing some kind of internal dissipation mechanism into the model equations.

As opposed to the numerical arguments given above, the physical necessity of considering internal dissipation terms is not so obvious. Tennekes (1978), for example, showed that in quasi-geostrophic flow the direct effect of small-scale eddies on larger scales is inversely proportional to the scale separation. The effect of subgrid scales on scales > 1000 km is in principle negligible, at least in short-range numerical weather prediction models, provided a reasonable resolution, say 100 km, is used. This is why direct dissipation of these scales should be avoided and confined to those scales for which there are fictitious sources such as aliasing, time decoupling or parameterized subgrid-scale fluxes.

Two generally applied scale selective methods are:

- The non-linear *eddy diffusion* method based upon certain physical concepts of the interaction of grid- and subgrid-scale processes. A typical example is the classical approach of Smagorinsky (1963) relating internal dissipation to the local deformation of the flow.
- The *filtering* method which prevents the accumulation of small-scale energy through the application of a numerical low-pass filter to the prognostic variables of the model equations (Shuman, 1957; Shapiro, 1971; Storch, 1980).

The scale selectivity of these methods was compared by Shapiro (1971) and Geleyn et al. (1977) by simply testing $u_{n+1} = u_n$ + diffusion and u_{n+1} = filtered u_n. Geleyn et al. found that fourth-degree non-linear diffusion schemes are more scale selective than second-degree ones, as might be expected from linear theory. Shapiro showed that high-order filter methods are superior to second-degree non-linear diffusion schemes. Equivalent results were obtained by Williamson (1978) in weather prediction experiments and Francis (1975) in general circulation simulations.

The present investigation compares second- and fourth-degree diffusion schemes with the filtering technique in a hemispheric model (Roeckner, 1979) which prevents systematic build-up of small-scale energy due to aliasing by using "Arakawa-type" approximations for the non-linear momentum advection terms (Arakawa and Lamb, 1977). Consequently, the horizontal eddy diffusion coefficients used are smaller than in Williamson's (1978) experiments and the interval between two successive filter applications is larger than in Francis' (1975) experiments. The results obtained from hemispheric 5-day forecast experiments are discussed mainly with respect to the spectral behaviour of kinetic and available potential energy.

Though our investigations cover only a period of 5 days, it seems probable to us that the results are also valid for longer periods.

2 The model

a *Equations*

The governing equations in a $(\lambda, \varphi, \sigma)$-coordinate system may be written schematically as follows

$$\left.\begin{aligned}(\pi u)_t + \ldots &= F_{\lambda V} + F_{\lambda H}\\ (\pi v)_t + \ldots &= F_{\varphi V} + F_{\varphi H}\\ (\pi T)_t + \ldots &= F_{TV} + F_{TH} + S_T\\ (\pi q)_t + \ldots &= F_{qV} + F_{qH} + S_q\\ \pi_t + \ldots &= \sigma\end{aligned}\right\} \qquad (1)$$

where u, v denote horizontal wind components, T temperature, q water vapour mixing ratio, and π difference between the pressures at the surface p_s and at the top of the model p_T. Advection, Coriolis and other terms belonging to the adiabatic system are omitted for convenience because their exact formulation is irrelevant to the problem under discussion. The F-terms at the right-hand side of (1) represent the effect of subgrid eddy fluxes of momentum ($F_{\lambda V}$, $F_{\lambda H}$, $F_{\varphi V}$, $F_{\varphi H}$), heat (F_{TV}, F_{TH}) and water vapour (F_{qV}, F_{qH}), where the subscripts V and H denote vertical and horizontal fluxes, respectively, and S_T and S_q represent sources/sinks of enthalpy and water vapour.

b *Discretization*

A detailed description of the finite-difference scheme used is given by Roeckner (1979), therefore, a summary should be sufficient here.

The model equations (1) are discretized on the so-called B-grid (Arakawa and Lamb, 1977) with $\Delta\lambda = \Delta\varphi = 2.8°$ and $3\Delta\sigma$-layers of equal depth. For time integration, a leapfrog scheme is used combined with a weak time filter (Asselin, 1972) with the coefficient equal to 0.005, which is sufficient to prevent time-decoupling.

To avoid a reduction of the time step $\Delta t = 4$ min because of the convergence of meridians near the Pole, the spatial prognostic variables polewards of 60°N are routinely Fourier-filtered. Spatial derivatives are approximated in a way similar to that of Arakawa (1972). Apart from time truncation, the following integral constraints are conserved in the discrete system:

- kinetic energy and an enstrophy-analogue in momentum advection,
- mean variances of temperature and mixing ratio in their corresponding advection terms,
- potential temperature and its variance during vertical advection,
- mass, momentum and total energy in the adiabatic system.

c *Boundaries*

Mountains are included in a realistic but slightly smoothed way. The top of the model is at $p_T = 100$ mb. The "vertical velocity" $\dot{\sigma} = d\sigma/dt$ vanishes at $p = p_T$

and $p = p_s$. The calculations are confined to the Northern Hemisphere with symmetric boundary conditions at the equator.

d *Subgrid-Scale Processes*

The experiments discussed in the next section were performed without considering radiation. Condensation and vertical subgrid-scale fluxes of momentum, heat and water vapour due to turbulence and convection are included. Details are given by Roeckner (1979).

e *Initial Data*

Initial conditions are for 2 January 1974, 00 GMT. Surface pressure and temperature analyses of the German Weather Service are used to obtain the mass field in the σ-system. The wind field was generated by dynamical initialization. Relative humidity was assumed to be 70% everywhere. Surface values of temperature (climatological) and humidity were kept constant in time, with 70% relative humidity over land and 100% over the oceans.

3 Methods

In the case of horizontal diffusion, the effect of subgrid-scale fluxes $F_{\lambda H}$, $F_{\varphi H}$, F_{TH} and F_{qH} in (1) is approximated by second- or fourth-degree finite-difference operators. Applying diffusion terms to the model equations modifies a certain state s to $\hat{s}$ by

$$\hat{s} = s + \Delta t G(s) \tag{2}$$

where $G(s)$ denotes the proper diffusion formulation. We used the second-degree approach of Smagorinsky (1963), which essentially leads to the form:

$$G(s) = k_0^2 \nabla (l^2 D \nabla s). \tag{3}$$

where k_0 is a free parameter, l a characteristic length scale (grid distance) and D the deformation of the flow. Furthermore, we used the fourth-degree approach of Williamson (1978)

$$G(s) = k_0^2 \nabla^2 (l^4 D \nabla^2 s) \tag{4}$$

The finite-difference formulations of (3) and (4) on the B-grid are given in Appendix 1.

During the numerical integration of the system (1), the diffusion terms (3) and (4) were recalculated only every third time step.

The filtering method transforms a certain state s to $\hat{s}$ by a linear operation

$$\hat{s} = F \cdot s \tag{5}$$

where F denotes a two-dimensional numerical filter with the property $\lim_{l \to 0} F =$ identity. For more details see Appendix 2.

We have introduced two modifications to the usual method of applying filters in large-scale models (Francis, 1975; Wallington, 1962; Hunt, 1974):

- The prognostic variables π, πu, πv, πT and πq in (1) contain small-scale features determined by orography. In order to avoid imbalances in the mass field, the surface pressure is reduced to mean sea level before filtering and recalculated thereafter, a procedure which is performed in an exactly reversible way. For the same reason, the variables u, v, T and q are filtered instead of the variables in flux form. (A test filtering the potential temperature instead of T showed that the influence of orography on the small-scale feature is negligible.)
- To avoid overdamping and wasting computer time, the frequency of applying the filter is controlled by the small-scale energy production of the model. About every half hour, the kinetic energy of the highest resolved wavenumbers (here $k = 59, \ldots, 64$) is calculated, averaged over time (7 time steps) and height, at about 45° latitude. If a specified threshhold value is exceeded, the filter is applied once to both time-levels of the leapfrog scheme. The choice of the threshhold value is oriented to the initial value of the small-scale energy. The results are, however, not very sensitive to small changes in this value.

The mean filter application interval, during the 5-day experiment performed, was about 100 time steps. Thus, on an average, the filtering procedure including the check of the noise level took only about 5 percent of the computer time required for the diffusion terms.

4 Evaluation method

Kinetic and available potential energy and some terms in the kinetic energy equation, such as dissipation and production, were calculated in zonal wavenumber space on pressure surfaces (Hinrichsen, 1977). The spectral distributions shown in the figures refer to hemispheric and daily averages (every 6 h) at the 500-mb level.

For the kinetic energy spectra, a -3 slope is predicted by two-dimensional theory (Charney, 1971) and verified by atmospheric data (Desbois, 1975; Chen and Wiin-Nielsen, 1978). For the available potential energy spectra, the theoretical -5 slope cannot be verified by observations. Chen and Wiin-Nielsen (1978), for example, found a -3 slope in the atmosphere between wavenumbers 10 and 40.

Therefore, the -3 slope beyond, say, wavenumber 10 will be used as a guide for judging the efficiency of the damping methods compared in the next section.

Differences occur in our experiments mainly in the smallest resolved scales and are small in the larger ones. On the other hand, the differences between our forecasts and the observed states after 5 days is fairly substantial with respect to the meteorologically relevant scales. Therefore, the verification was made not against observations but against a reference experiment lacking horizontal dissipation. This reference run allows estimation of the effect of the dissipation on the largest scales, which should be small.

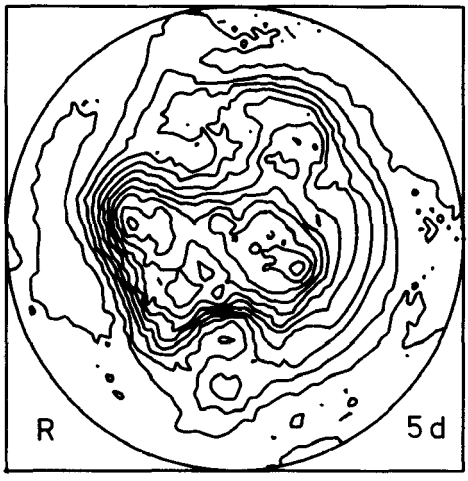

Fig. 1 Hemispheric distribution of 500-mb geopotential heights at forecast Day 5 for reference run R. Contour spacing: 80 m.

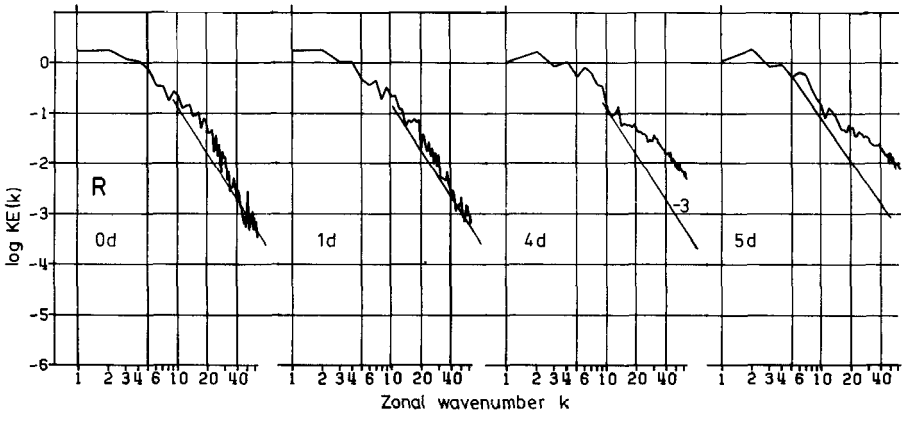

Fig. 2 Spectral kinetic energy (KE) distributions at 500-mb of the initial state and for Days 1, 4 and 5 averaged over 6-h intervals. Units: 10^5 J/(m^2 × 10^3 mb).

5 Results

a *Reference Run*

The reference run denoted by R was performed without horizontal diffusion or filtering. The solution remained stable for at least 5 days. However, small-scale noise developed and is superimposed on the large-scale patterns, (see Fig. 1). The unrealistic, but not dramatic, increase of noise is also evident in the spectral distribution of kinetic energy (Fig. 2). This noise mainly reflects the absence of an energy sink at small-scales and is generated by orography, the land-sea distribution, subgrid-scale processes similar to convection and the time truncation error. A spurious energy cascade due to aliasing is largely reduced by the Arakawa-type approximation used for the momentum advection terms.

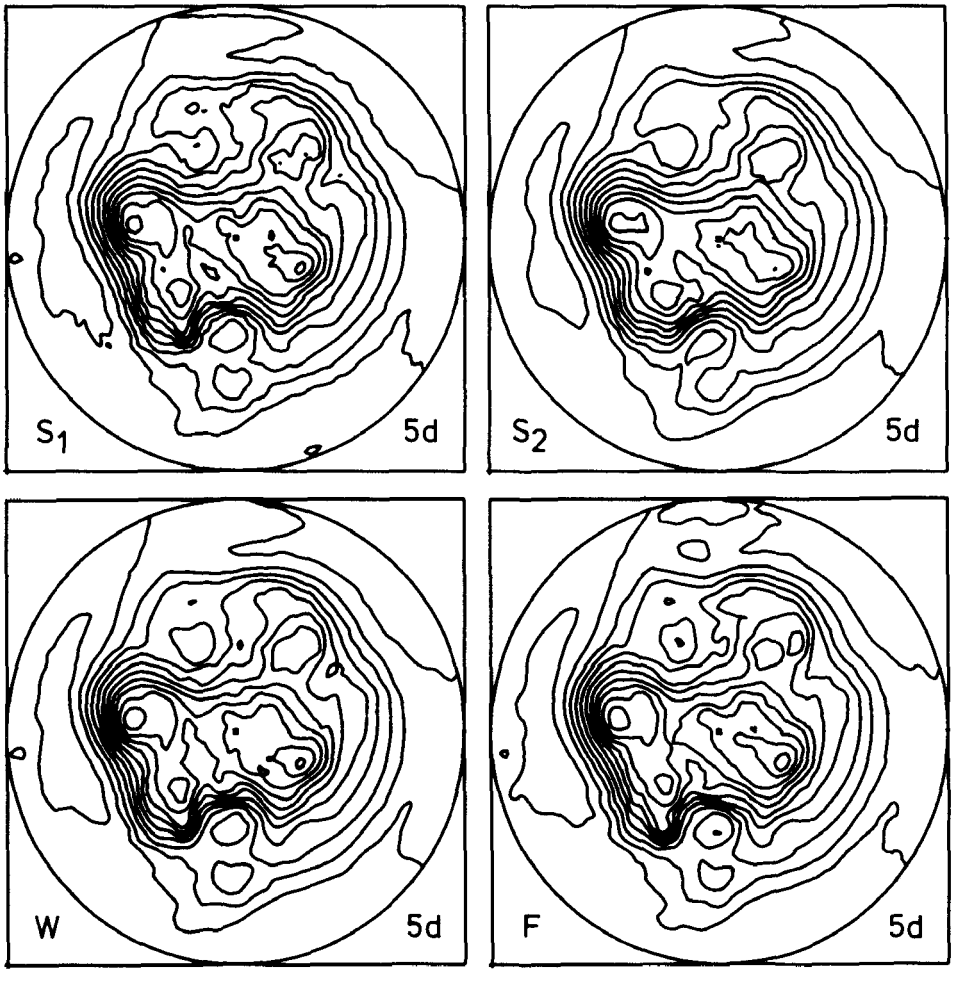

Fig. 3 As Fig. 1, except for experiments S_1, S_2, W and F.

b *Experiments*

In the following sections we shall compare experiments with the horizontal diffusion methods of Smagorinsky (1963) and Williamson (1978) and a numerical filter technique (Storch, 1978). The following notations will be used: S_1 for Smagorinsky's second-degree scheme with $k_0 = 0.1$ in (3), S_2 as for S_1 with $k_0 = 0.2$, W for Williamson's fourth-degree scheme with $k_0 = 0.1$ in (4), and F for Storch's seventh-order numerical filter (15 points each in zonal and meridional directions) applied according to the algorithm given in Section 3.

Figure 3 shows the 500-mb height fields after 5 days. Compared to the reference run R (Fig. 1), the fields are much smoother, yet the large-scale features are similar. The S_1-run is, however, noisier than the others and the S_2-run seems to be slightly oversmoothed. Some synoptic features are more sharply pronounced in F than in the other experiments.

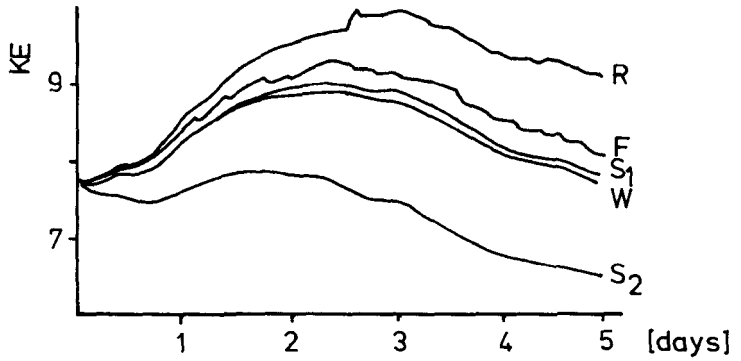

Fig. 4 Temporal development of space-averaged eddy kinetic energy. Units: 10^5 J/(m^2 × 10^3 mb).

c *Eddy Kinetic Energy*

The temporal development of mean eddy kinetic energy is shown in Fig. 4 for all experiments. S_1 and W give equivalent results, whereas S_2 shows a remarkable loss of energy. The weakest energy reduction with respect to R is to be seen in the filter experiment F.

d *Spectral Energy Distribution*

Figs 5 and 6 show the 500-mb spectral distribution of kinetic energy and available potential energy. The -3 power slope is drawn to facilitate comparison of the four experiments. The spectral slope is reproduced "correctly" by S_2 and W. S_1 produces a rather high level of small-scale energy, while F shows an excessive reduction beyond about wavenumber 40 because of the shape of the filter's response function (Storch, 1978). Differences at the large scale can hardly be detected in Figs 5 and 6. Therefore, additional information is given in Tables 1 and 2 for three large-scale spectral ranges. In the "long" waves (k = 1–4), there is a loss of energy compared to the reference run in all experiments except F, which shows practically no change. The same is true for the "short" waves (k = 9–15). However, the "cyclone-scale" waves (k = 5–8) reveal a general increase of available potential energy, which cannot be understood in terms of linear arguments.

S_2 shows a remarkable energy reduction at practically all ranges and differs considerably from the other experiments which are as a whole closer together. The smallest deviation from the reference run occurs in experiment F.

If only the total eddy kinetic energy is considered (Fig. 4), S_1 and W seem to be equivalent. Their corresponding spectral energy distributions, however, differ considerably (Figs 5, 6 and Tables 1, 2). More insight into the properties of the different diffusion schemes is obtained from analyses of the dissipation term in the kinetic energy equation as described in the next sub-section.

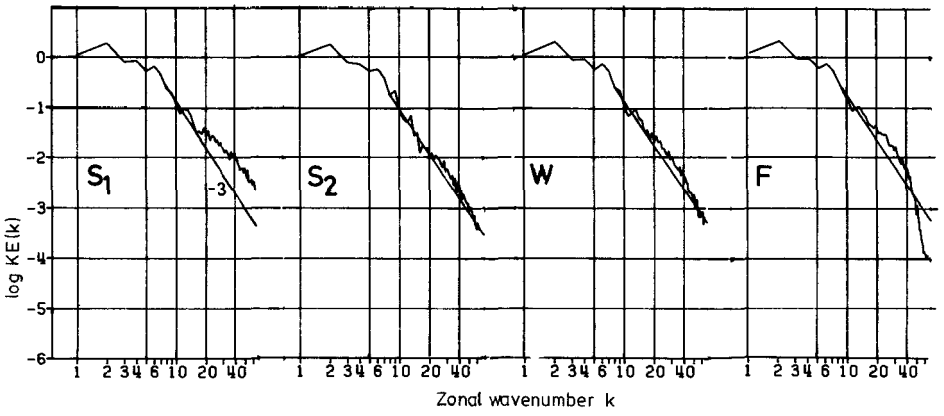

Fig. 5 Spectral kinetic energy distributions at 500-mb for Day 5 averaged over 6-h intervals. Units: 10^5 J/(m^2 × 10^3 mb).

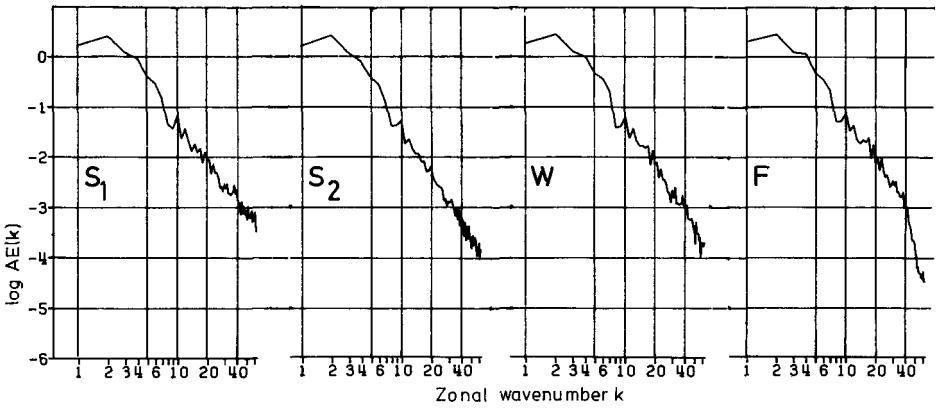

Fig. 6 As Fig. 5, except for available potential energy (AE).

TABLE 1. Percentage deviation of mean kinetic energy at 500 mb from the reference run for 3 wavenumber ranges at forecast Day 5 (6-h averages)

	k		
Experiment	1–4	5–8	9–15
S_1	−55.0	−5.4	−21.9
S_2	−15.1	−15.7	−46.6
W	−4.0	+2.8	−29.5
F	+0.02	+3.0	−15.5

TABLE 2. As Table 1, except for available potential energy

	k		
Experiment	1–4	5–8	9–15
S_1	−6.4	+5.2	−7.4
S_2	−9.6	+6.1	−25.3
W	−6.6	+24.0	−6.6
F	−2.1	+18.4	+3.1

TABLE 3. Initial 500-mb distribution of hemispherically-averaged dissipation due to horizontal diffusion, summed over several wavenumber ranges. Units: W/(m^2 × 10^3 mb)

		k				
Experiment	All Waves	1–4	5–8	9–15	16–32	33–64
S_1	0.377	0.148	0.063	0.075	0.078	0.013
S_2	1.508	0.592	0.251	0.298	0.312	0.052
W	0.409	0.108	0.061	0.082	0.115	0.043

TABLE 4. As Table 3, except for dissipation due to horizontal *and* vertical diffusion and Day 5 forecasts averaged over 6-h intervals

		k				
Experiment	All Waves	1–4	5–8	9–15	16–32	33–64
S_1	0.676	0.202	0.111	0.108	0.147	0.107
S_2	0.761	0.297	0.159	0.130	0.119	0.056
W	0.609	0.152	0.089	0.104	0.168	0.097

e *Energetics*

The transformation terms in the kinetic energy equation (dissipation, production, non-linear interaction, fluxes) were calculated on pressure surfaces in zonal wavenumber space according to Hinrichsen (1977).

Table 3 shows the initial spectral distribution of the mean 500-mb dissipation term calculated from the horizontal diffusion terms (3) and (4) for the experiments S_1, S_2 and W. Although the same constant, $k_0 = 0.1$, was used for S_1 and W, giving a mean eddy diffusion coefficient at 500-mb of 2.1×10^4 m^2 s^{-1}, the total dissipation (first column) varies slightly owing to the different formulations of second- and fourth-degree diffusion in (3) and (4), respectively (see also Appendix 1). Even though the total dissipations of S_1 and W are similar, their spectral distributions are different: In the ranges $k = 1$–4 and $k =$ 5–8 the W-scheme produces less dissipation, whereas in the range $k = 33$–64 it is comparable with the second degree scheme S_2 which uses $k_0 = 0.2$.

On Day 5 the situation in the high wavenumber range is reversed. Table 4, which contains the sum of horizontal and vertical dissipations (unfortunately, due to a coding error, Table 4 includes vertical dissipation, which amounts to

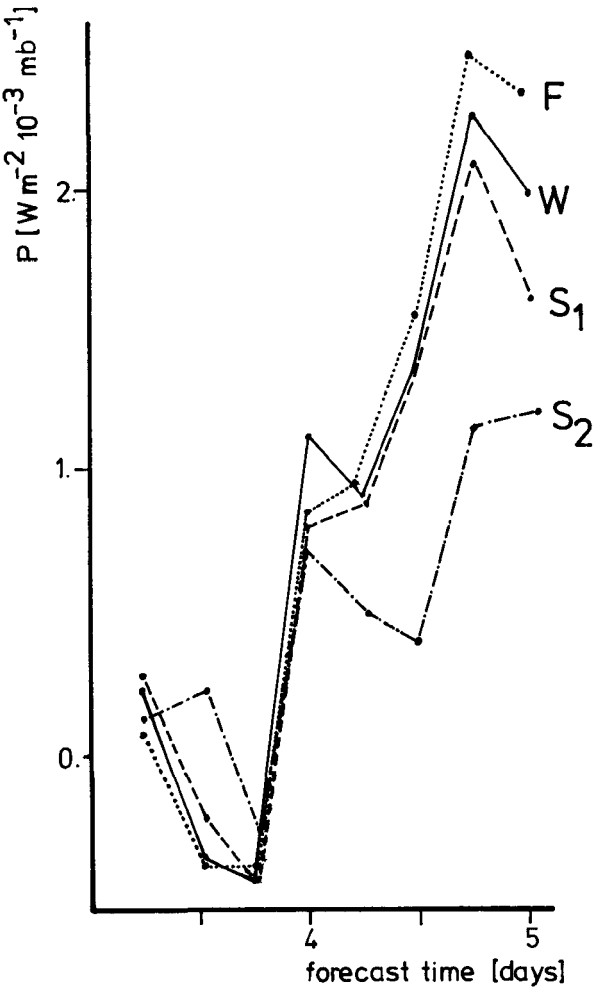

Fig. 7 Temporal development of the mean wavenumber 2 production term at 500-mb. Units: W/(m^2 × 10^3 mb).

about 50% of the total internal dissipation given in the Table), shows that for k = 33–64, S_2 gives the weakest dissipation and S_1 the highest. In the long waves, S_2 still shows the strongest dissipation, however, the difference with respect to S_1 and W has decreased with time.

The striking differences observed in the kinetic energy of the relevant scales k = 1–15 between S_2 and the other experiments (Table 1) cannot be fully explained by the repeated application of an excessively high diffusion term which has the tendency to gradually adjust to a reasonable value (Tables 3 and 4).

Beyond about Day 3, other terms in the kinetic energy equation, such as production, gradually became reduced in experiment S_2. The most remarkable feature during the last two days of the experiments was an increase of the wavenumber 2 production term, shown in Fig. 7. Except for S_2, all experiments including the reference run (not shown) gave equivalent results. The

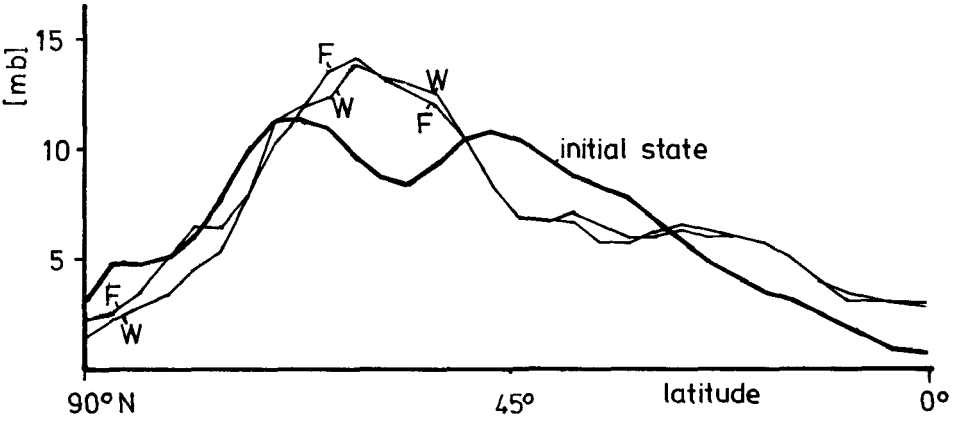

Fig. 8 Meridional distribution of zonal standard deviation of surface pressure at Day 5. Units: mb.

reduction of the S_2-production term may be explained by an oversmoothing of the long waves during the first period of integration.

f *Meridional Distribution*

Until now, only the zonal structure of the energy terms has been investigated. We also compared zonal averages and standard deviations of several variables as functions of latitude. As a whole, the experiments gave similar results, exemplified by the meridional distribution of the standard deviation of surface pressure (Fig. 8). It is especially noteworthy that the filter experiment F produced no irregularities in the polar region. This might have been expected as a result of cross-polar filtering (Appendix 2).

6 Conclusions

The main conclusions to be drawn from comparing horizontal diffusion and filtering methods in 5-day simulations with an Arakawa-type model are:

- As might be expected, fourth-degree non-linear diffusion schemes are superior to those of second-degree from the viewpoint of scale selectivity. For a given amount of high wavenumber dissipation needed to produce a realistic spectral slope, fourth-degree schemes lead to less damping in the relevant scales than second-degree schemes.

  A similar result was obtained by Williamson (1978) with a model which contains non-Arakawa-type approximations of the non-linear terms.
- A high order two-dimensional numerical filter applied intermittently, depending on the model's noise production, is sufficient to avoid a build-up of energy at the small-scale end of the spectra. The results of the filter and fourth-degree diffusion experiments are essentially equivalent, although the filter appears to be slightly more scale selective. Apart from its scale selectivity, the main advantage of the filter is its computational economy which results from intermittent application. For example, during our 5-day

experiments the total computer time required to calculate the filtering procedure took only about 5 percent of the time for the fourth-degree diffusion terms.

- Overdamping at low wavenumbers may lead to a gradual decrease of kinetic energy production from available potential energy. This fact might be important for long-term integration.

Appendix 1

a *Second-Degree Diffusion (Smagorinsky, 1963)*

The eddy diffusion terms for momentum, temperature and humidity are approximated in the B-grid as follows:

$$F_{\lambda H} = r^{-1}[\delta_\lambda(\bar{K}_2^\varphi \bar{D}_T^\varphi \bar{\pi}^\varphi) + \delta_\varphi(\bar{K}_2^\lambda \bar{D}_S^\lambda \bar{\pi}^\lambda \cos\varphi)] \tag{A1}$$

$$F_{\varphi H} = r^{-1}[\delta_\lambda(\bar{K}_2^\varphi \bar{D}_S^\varphi \bar{\pi}^\varphi) - \delta_\varphi(\bar{K}_2^\lambda \bar{D}_T^\lambda \bar{\pi}^\lambda \cos\varphi)] \tag{A2}$$

$$F_{TH} = r^{-1}[r^{-1}\delta_\lambda(\bar{K}_2^\lambda \bar{\pi}^\lambda (\overline{T/\theta}^\lambda)\delta_\lambda\theta) + a^{-1}\delta_\varphi(\bar{K}_2^\varphi \bar{\pi}^\varphi (\overline{T/\theta}^\varphi)\delta_\varphi\theta \cos\varphi)] \tag{A3}$$

$$F_{qH} = r^{-1}[r^{-1}\delta_\lambda(\bar{K}_2^\lambda \bar{\pi}^\lambda \delta_\lambda q) + a^{-1}\delta_\varphi(\bar{K}_2^\varphi \bar{\pi}^\varphi \delta_\varphi q \cos\varphi)] \tag{A4}$$

with $D_T = r^{-1}[\delta_\lambda \bar{u}^\varphi - \delta_\varphi(\bar{v}^\lambda \cos\varphi)]$

$D_S = r^{-1}[\delta_\lambda \bar{v}^\varphi + \delta_\varphi(\bar{u}^\lambda \cos\varphi)]$

$K_2 = k_0^2 l^2 D$

$l^2 = a^2 \cos\varphi \, \Delta\lambda \Delta\varphi$

and $D = (D_T^2 + D_S^2)^{1/2}$

and the following notation: λ, φ are longitude, latitude, $\Delta\lambda$, $\Delta\varphi$ are increments, $r = a \cdot \cos\varphi$, and a is mean Earth radius, u, v are zonal and meridional wind components, T, q are temperature and humidity, θ is potential temperature, $\pi = p_s - p_T$, and p_s is surface pressure and p_T, pressure at the top of the model, and k_0 is a proportionality constant,

$$\delta_x A = [A(x + \Delta x/2) - A(x - \Delta x/2)]/\Delta x$$

$$\bar{A}^x = [A(x + \Delta x/2) + A(x - \Delta x/2)]/2$$

b *Fourth-Degree Diffusion (Williamson, 1978)*

Apart from the higher order derivative, the fourth-degree scheme has been simplified slightly compared to the second-order scheme:

$$F_{\lambda H} = -(\Delta\bar{\pi}^{\lambda\varphi}\bar{K}_4^{\lambda\varphi}\Delta)u \tag{A5}$$

$$F_{\varphi H} = -(\Delta\bar{\pi}^{\lambda\varphi}\bar{K}_4^{\lambda\varphi}\Delta)v \tag{A6}$$

$$F_{TH} = -(\Delta\pi K_4(T/\theta)\Delta)\theta \tag{A7}$$

$$T_{qH} = -(\Delta\pi K_4\Delta)q \tag{A8}$$

with $K_4 = k_0^2 D$

and $\Delta\psi = \delta_\lambda\delta_\lambda\psi + (\cos\varphi)^{-1}\delta_\varphi(\delta_\varphi\psi \cos\varphi)$

Appendix 2

Design of Hemispheric Numerical Filters

Starting with a one-dimensional numerical filter of order m with weights $a_0, \ldots, a_m$ as given by Storch (1978), one can define a "meridional filter" T_φ and a "zonal filter" T_λ by:

$$(T_\varphi f)(\varphi,\lambda) = \begin{cases} a_0 f(\varphi,\lambda) + \sum_{j=1}^{m} a_j [f(\varphi - j\Delta\varphi,\lambda) + f(\varphi + j\Delta\varphi,\lambda)] & \text{if } \varphi \neq \pi/2 \\ \text{zonal mean of } (T_\varphi f)\left(\frac{\pi}{2} - \Delta\varphi, \lambda\right) & \text{if } \varphi = \pi/2 \end{cases}$$

$$(T_\lambda f)(\varphi,\lambda) = \begin{cases} a_0 f(\varphi,\lambda) + \sum_{j=1}^{m} a_j [f(\varphi,\lambda - j\Delta\lambda) + f(\varphi,\lambda + j\Delta\lambda)] & \text{if } \varphi \neq \pi/2 \\ f(\varphi,\lambda) & \text{if } \varphi = \pi/2 \end{cases}$$

In order to apply these formulae to all grid points one has to extend the function f to be filtered outside the domain $[0, (\pi/2)] \times [0, 2\pi]$. For the zonal direction this is done periodically, i.e. $f(\varphi,\lambda + 2\pi) = f(\varphi,\lambda)$.

At the equator (i.e. $\varphi - m\Delta\varphi < 0$) one has to look at the boundary conditions. If they are symmetric the extension is

$$f(-\varphi,\lambda) = \begin{cases} f(\varphi,\lambda) \text{ for scalar fields and the } \lambda\text{-component of the velocity} \\ -f(\varphi,\lambda) \text{ for the } \varphi\text{-component of the velocity} \end{cases}$$

When crossing the Pole (i.e. $\varphi + m\Delta\varphi > \pi/2$) the signs of the velocity components are reversed, leading to

$$f\left(\frac{\pi}{2} + \varphi,\lambda\right) = \begin{cases} f(\pi/2 - \varphi,\lambda + \pi) \text{ for scalar fields} \\ -f(\pi/2 - \varphi,\lambda + \pi) \text{ for the velocity components.} \end{cases}$$

The two-dimensional hemispheric filter F is simply defined as $F = T_\lambda \cdot T_\varphi$. It can be shown that $T_\lambda \cdot T_\varphi = T_\varphi \cdot T_\lambda$ (Storch, 1980).

Acknowledgements

We thank Dr K. Hinrichsen for preparing the energetics procedure, Mr G. W. Fischer for handling the data and Professor Dr G. Fischer and Dr Z. Janjić for a critical review of the manuscript.

This research was supported by the Deutsche Forschungsgemeinschaft, Federal Republic of Germany.

References

ARAKAWA, A. 1972. Design of the UCLA general circulation model. Tech. Rep. No. 7, Dep. of Meteorology, University of California, Los Angeles, 116 pp.

——— and V.R. LAMB. 1977. Computational design of the basic dynamical processes of the UCLA general circulation model. *Methods Comput. Phys.* **17**: 174–265.

ASSELIN, R. 1972. Frequency filter for time integration. *Mon. Weather Rev.* **100**: 487–490.

CHARNEY, J.G. 1971. Geostrophic turbulence. *J. Atmos. Sci.* **28**: 1087–1095.

CHEN, T.C. and A. WIIN-NIELSEN. 1978. On nonlinear cascades of atmospheric energy and enstrophy in a two-dimensional spectral index. *Tellus*, **30**: 313–322.

DESBOIS, M. 1975. Large-scale kinetic energy spectra from Eulerian analysis of EOLE wind data. *J. Atmos. Sci.* **32**: 1838–1847.

FRANCIS, P.E. 1975. The use of a multipoint filter as a dissipative mechanism in a numerical model of the general circulation of the atmosphere. *Quart. J. R. Meteorol. Soc.* **101**: 567–582.

GELEYN, F.F.; A. HOLLINGWORTH, J.F. LOUIS and M. TIEDTKE. 1977. Parameterization studies at ECMWF. GARP-Report No. 15, pp. 68–75.

HINRICHSEN, K. 1977. Development of a spectral and spatial hemispheric energetics procedure. GARP-Report No. 15, pp. 64–66.

HUNT, B.G. 1974. A global general circulation model of the atmosphere based on the semispectral method. *Mon. Weather Rev.* **102**: 3–16.

ROECKNER, E. 1979. A hemispheric model for short range numerical weather prediction and general circulation studies. *Beitr. Phys. Atmos.* **52**: 262–287.

SHAPIRO, R. 1971. The use of linear filtering as a parameterization of atmospheric diffusion. *J. Atmos. Sci.* **58**: 523–531.

SHUMAN, F.G. 1957. Numerical methods in weather prediction: II. Smoothing and filtering. *Mon. Weather Rev.* **85**: 357–361.

SMAGORINSKY, J. 1963. General circulation experiments with the primitive equations: I. The basic experiment, *Mon. Weather Rev.* **91**: 99–164.

STORCH, H.V. 1978. Construction of optimal numerical filters fitted for noise damping in numerical simulation models, *Beitr. Phys. Atmos.* **51**: 189–197.

———. 1980. Numerische Filter zur Dämpfung meteorologischen Lärms in hemisphärischen Modellen. Hamburger Geophysikalische Einzelschriften **44**: Hamburg, 96 pp.

TENNEKES, H. 1978. Turbulent flow in two and three dimensions. *Bull. Am. Meteorol. Soc.* **59**: 22–28.

WALLINGTON, C.E. 1962. The use of smoothing or filtering operators in numerical forecasts. *Quart. J. R. Meterol. Soc.* **88**: 470–484.

WILLIAMSON, D.L. 1978. The relative importance of resolution, accuracy and diffusion in short range forecasts with the NCAR global circulation model, *Mon. Weather Rev.* **106**: 69–88.